Available online at www.sciencedirect.com
SCIENCE DIRECT®
International Journal of Thermal Sciences 45 (2006) 982–989
International Journal of Thermal Sciences
www.elsevier.com/locate/ijts

Lattice Boltzmann method simulation of a cylinder in the backward-facing step flow with the field synergy principle

Chao-Kuang Chen *, Tzu-Shuang Yen, Yue-Tzu Yang

Department of Mechanical Engineering, National Cheng Kung University, Tainan, 70101, Taiwan

Received 4 October 2005; received in revised form 22 December 2005; accepted 22 December 2005

Available online 30 January 2006

Abstract

In this paper, the Lattice Boltzmann Method (LBM) is applied to simulate incompressible steady low Reynolds number backward-facing step flows. The investigated Reynolds number range is limited to a maximum value of $Re = 200$. The field synergy principle is applied to demonstrate that the increased interruption within the fluid caused by the introduction of the cylinder will reduce the intersection angle between the velocity vector and the temperature gradient. Furthermore, the numerical results compare with the experiment data and confirm the relationship between the velocity vector and temperature gradient predicted by the field synergy principle.

Keywords: Lattice Boltzmann method; Backward-facing step; Heat transfer; Field synergy principle

1. Introduction

In recent years, the Lattice Boltzmann Method (LBM) has emerged as an alternative, computational technique for simulating fluid flows and modeling the physics of fluids [1]. The macroscopic method for computational fluid dynamics (CFD) is usually solving the Navier–Stokes equations to obtain the velocity and pressure fields. But the LBM is based on microscopic models and mesoscopic kinetic equations. These algorithms attempt to model a fluid by simulating a discretized single-particle phase space distribution function similar to that described by the traditional Boltzmann equation. The LBM numerically solves the kinetic equation (the Boltzmann BGK equation) for the single-particle distribution function. The fundamental concept of the LBM is to construct simplified kinetic models which incorporate the essential physics of microscopic or mesoscopic processes such that the macroscopic averaged properties obey the desired macroscopic equations.

The use of the Lattice Boltzmann equation as a numerical scheme was first proposed by McNamara and Zanetti [2]. This equation neglects the motion of individual particles and results in a smooth macroscopic behavior. Higuera et al. [3,4] introduced a linearized collision operator to simplify the scheme and eliminate statistical noise. A particularly simple linearized version of the collision operator is the Bhatnagar–Gross–Krook collision operator [5], which uses a single relaxation time parameter. The relaxation term is known as the BGK operator and the corresponding model is referred to as the Lattice Boltzmann BGK model. The BGK collision operator greatly accelerates the computation process. Due to its extreme simplicity, the Lattice BGK (LBGK) equation [6,7] has emerged as the most widely employed version of the Lattice Boltzmann model.

Since the method typically uses uniform regular Cartesian lattices in space, curved boundaries are generally approximated by a series of stairs. However, this approximation leads to a reduction in the computational accuracy. Accordingly, an approach for curved walls has recently been proposed by Filippova and Hanel [8] based on an improvement of the bounce-back rule. The numerical stability was further improved by Mei et al. [9] with a revision expression for $\Delta < \frac{1}{2}$. Guo [10] extended the extrapolation scheme proposed by Chen et al. [11] to develop a new treatment for curved boundaries.

The study of backward-facing step flow constitutes an important branch of fundamental fluid mechanics. The interest in

* Corresponding author. Tel.: +886 6 275 7575 ext. 62140; fax: +886 6 234 2081.
E-mail address: ckchen@mail.ncku.edu.tw (C.-K. Chen).

1290-0729/$ – see front matter
doi:10.1016/j.ijthermalsci.2005.12.009

Nomenclature

c	lattice streaming speed
c_s	speed of sound
c_p	specific heat capacity
g_α	energy distribution function
ER	channel expansion ratio, H/h
f_α	density distribution function
f_α^{eq}	equilibrium distribution function for f_α
g_α^{eq}	equilibrium distribution function for g_α
H	channel width downstream of step
h	step height
k	thermal conductivity
Nu	Nusselt number
$\overline{Nu}$	average Nusselt number
Pr	Prandtl number
p	pressure
Re	Reynolds number
T	temperature
U	maximum velocity in inlet
$\vec{V}$	velocity vector
X_R	reattachment location

Greek symbols

τ_v	relaxation time for f_α
τ_c	relaxation time for g_α
ε	internal energy
χ	diffusivity
ρ	density
ν	kinematic viscosity
δ	small parameter
δx	lattice spacing
δt	time step
θ	intersection angle between velocity and temperature gradient

Subscripts

m	mean
w	wall

such a flow was intensified with the experimental and numerical work of Armaly et al. [12]. They presented a detail experimental investigation in a backward-facing step geometry for an expansion ratio $ER = 1.9423$ and Reynolds numbers up to $Re = 8000$. The main characteristic of flows of this type is the formation of a recirculation region immediately downstream of the step. This flow pattern has a large number of practical engineering applications, including airfoils, electrical devices, diffusers, and combustors. Kondoh [13] used a traditional CFD method to simulate laminar heat transfer in a separating and reattaching flow. The numerical results were found to be in good agreement with the experimental data of Aung [14] and Hall [15].

Drawing an analogy between heat convection and heat conduction, Guo [16] and Wang [17] studied the mechanisms of convective heat transfer and proposed a novel approach for enhancing convective heat transfer under a parabolic fluid flow structure. The convection term can be transformed into a dot product of the velocity vector and the temperature gradient. The convective heat transfer can be enhanced by raising the value of the integral of convective term over the thermal boundary layer. This novel approach was aimed at improving the uniformity of the velocity and temperature profiles and reducing the intersection angle between the dimensionless velocity vector and the temperature gradient. Guo [16] referred to this approach as the field synergy (coordination) principle and Tao [18,19] extended the concept from parabolic to elliptic fluid flows and to other transport phenomena. Guo [20] defined the field synergy number as an indication of the synergy degree between velocity and temperature field for the entire flow and heat transfer domain.

The objective of this study is to analyze the velocity and temperature fields of incompressible steady low Reynolds number backward-facing step flows. The flow is investigated both with and without the insertion of the cylinder downstream from the step. The computed results are then compared with the published experimental and numerical results.

2. Lattice Boltzmann equations

2.1. Lattice Boltzmann equations for density and velocity fields

This study simulates the steady backward-facing step flow using the 9-velocity LBM model with a 2D square lattice, designated the D2Q9 model. In this model, $c = \delta x/\delta t = \delta y/\delta t$ is the lattice streaming speed and δx and δy are the grid spacings in the x- and y-directions, respectively, and correspond to the distance which a particle moves in each time step of the LBM simulation. The discrete velocities for the D2Q9 model are defined as:

$$\begin{aligned} &\vec{e}_\alpha = (0,0), && \alpha = 0, \text{ rest particle} \\ &\vec{e}_\alpha = (\pm c, 0), (0, \pm c), && \alpha = 1,2,3,4 \\ &\vec{e}_\alpha = (\pm c, \pm c), && \alpha = 5,6,7,8 \end{aligned} \tag{1}$$

The governing equation for the density distribution function is given by:

$$f_\alpha(\vec{x} + \vec{e}_\alpha \delta t, t + \delta t) - f_\alpha(\vec{x}, t) = -\frac{1}{\tau_v}\left[f_\alpha(\vec{x}, t) - f_\alpha^{\mathrm{eq}}(\vec{x}, t)\right] \tag{2}$$

where τ_v characterizes the relaxation time of the density distribution function towards the local equilibrium f_α^{eq}. The equilibrium density distribution is expressed as:

$$f_\alpha^{\mathrm{eq}} = w_\alpha \rho \left[1 + \frac{3\vec{e}_\alpha \cdot \vec{V}}{c^2} + \frac{9}{2}\frac{(\vec{e}_\alpha \cdot \vec{V})^2}{c^4} - \frac{3}{2}\frac{\vec{V}^2}{c^2}\right] \tag{3}$$

$$w_0 = \frac{4}{9}, \quad w_\alpha = \frac{1}{9} \quad \text{for } \alpha = 1, 2, 3, 4$$

$$w_\alpha = \frac{1}{36} \quad \text{for } \alpha = 5, 6, 7, 8$$

The macroscopic density and velocity are calculated from:

$$\rho = \sum_\alpha f_\alpha \tag{4}$$

$$\rho \vec{V} = \sum_\alpha \vec{e}_\alpha f_\alpha \tag{5}$$

Adopting the same procedure as that employed by Hou et al. [21], the continuity and Navier–Stokes equations can be derived through the Chapman–Enskog expansion of the density distribution function. The details of this derivation are provided in [21]. The Navier–Stokes equation and continuity equation are then given by:

$$\partial_t \rho + \nabla \cdot (\rho \vec{V}) = 0 \tag{6}$$

$$\partial_t (\rho \vec{V}) + \nabla \cdot (\rho \vec{V} \vec{V}) = -\nabla p + \nu \left[\nabla^2 (\rho \vec{V}) + \nabla \left(\nabla \cdot (\rho \vec{V}) \right) \right] \tag{7}$$

where $p = c_s^2 \rho$ is the pressure, derived from the equation of state for an ideal gas, $c_s = c/\sqrt{3}$ is the speed of sound, and the kinematic viscosity is given by:

$$\nu = \frac{(2\tau_\nu - 1)}{6} \frac{(\delta x)^2}{\delta t} \tag{8}$$

The Mach number is defined as $M = \vec{V}/c_s$. A low Mach number assumption can be invoked as the nearly incompressible limit is approached, i.e. $M \ll 1$. The incompressible continuity equation and Navier–Stokes equation are expressed as:

$$\nabla \cdot \vec{V} = 0 \tag{9}$$

$$\partial_t \vec{V} + \vec{V} \cdot \nabla \vec{V} = -\frac{\nabla p}{\rho} + \nu \nabla^2 \vec{V} \tag{10}$$

2.2. Lattice Boltzmann equation for temperature field

In general, previous thermal Lattice Boltzmann models fall into two distinct categories: the multi-speed approach [22] and the double distribution function models [23,24]. The multi-speed approach is a straightforward extension of the isothermal model, but suffers severe numerical instability and it needs a large set of discrete velocities. The temperature variation is limited to a narrow range and a fixed Prandtl number. The passive scalar approach [23] utilizes the fact that the macroscopic temperature satisfies the same evolution equation as a passive scalar. However, it neglects viscous heat dissipation and the compression work done by pressure. Finally, although the thermal energy distribution model [24] is an adequate tool for solving real thermal problems, it suffers a number of shortcomings. For example, it contains a complicated gradient operator term in the evolution equation for the temperature, and hence the simplicity characterizing the LBM is lost. Furthermore, since viscosity is involved not only in the momentum equation, but also in the energy equation, additional variables for the thermal energy distribution function must be introduced in order to ensure that the viscosity remains consistent in the governing equations of the thermal energy distribution model and to avoid implicitness of the schemes [24]. Consequently, the current study employs the simplified thermal model proposed by Peng et al. [25] for simulation purposes. This model considers that the compression work done by the pressure and the viscous heat dissipation can be neglected for incompressible flow, and hence the gradient term used to recover these terms through the Chapman–Enskog expansion can be dropped from the evolution equation.

The governing equation of the simplified thermal energy distribution model is given by:

$$g_\alpha(\vec{x} + \vec{e}_\alpha \delta t, t + \delta t) - g_\alpha(\vec{x}, t) = -\frac{1}{\tau_c} \left[g_\alpha(\vec{x}, t) - g_\alpha^{\text{eq}}(\vec{x}, t) \right] \tag{11}$$

According to He et al. [24], the equilibrium energy distribution functions, g, can be written as:

$$g_0^{\text{eq}} = -\frac{2\rho\varepsilon}{3} \frac{\vec{V}^2}{c^2} \tag{12}$$

$$g_{1,2,3,4}^{\text{eq}} = \frac{\rho\varepsilon}{9} \left[\frac{3}{2} + \frac{3}{2} \frac{\vec{e}_\alpha \cdot \vec{V}}{c^2} + \frac{9}{2} \frac{(\vec{e}_\alpha \cdot \vec{V})^2}{c^4} - \frac{3}{2} \frac{\vec{V}^2}{c^2} \right] \tag{13}$$

$$g_{5,6,7,8}^{\text{eq}} = \frac{\rho\varepsilon}{36} \left[3 + 6 \frac{\vec{e}_\alpha \cdot \vec{V}}{c^2} + \frac{9}{2} \frac{(\vec{e}_\alpha \cdot \vec{V})^2}{c^4} - \frac{3}{2} \frac{\vec{V}^2}{c^2} \right] \tag{14}$$

where $\varepsilon = DRT/2$, in which R is the gas constant and D is the dimension. The macroscopic temperature can then be calculated by:

$$\rho\varepsilon = \sum_\alpha g_\alpha \tag{15}$$

Using the procedure presented by Hou et al. [21], the Chapman–Enskog expansion for the new thermal energy distribution function can be used to recover the macroscopic energy equation. Using $g_\alpha^{(0)}$ rather than g_α^{eq}, and expanding g_α about $g_\alpha^{(0)}$, it can be shown that:

$$g_\alpha = g_\alpha^{(0)} + \delta g_\alpha^{(1)} + \delta^2 g_\alpha^{(2)} + \mathrm{O}(\delta^3) \tag{16}$$

where δ is the expansion parameter. To investigate changes in different time scales, t_0 and t_1 are introduced as $t_0 = t$, $t_1 = \delta t, \ldots$; such that:

$$\partial_t = \partial_{t0} + \delta \partial_{t1} + \delta^2 \partial_{t2} + \cdots \tag{17}$$

The first-order expansion of Eq. (11) is:

$$(\partial_{t0} + \vec{e} \cdot \nabla) g_\alpha^{(0)} = -\frac{1}{\tau_c} g_\alpha^{(1)} \tag{18}$$

The second-order expansion of Eq. (11) is:

$$\partial_{t1} g_\alpha^{(0)} + \left(1 - \frac{1}{2\tau_c} \right) (\partial_{to} + \vec{e} \cdot \nabla) g_\alpha^{(1)} = -\frac{1}{\tau_c} g_\alpha^{(2)} \tag{19}$$

Summing Eqs. (18) and (19) gives:

$$\partial_{t0}(\rho\varepsilon) + \nabla \cdot (\rho \vec{V} \varepsilon) = 0 \tag{20}$$

$$\partial_{t1}(\rho\varepsilon) + \left(1 - \frac{1}{2\tau_c} \right) \Pi^{(1)} = 0 \tag{21}$$

where $\Pi^{(1)} = -\frac{2}{3}\tau_c \nabla^2(\rho\varepsilon)$. Combining Eqs. (20) and (21), the energy equation can be obtained as:

$$\partial_t(\rho\varepsilon) + \nabla\cdot(\rho\vec{V}\varepsilon) = \chi\nabla^2(\rho\varepsilon) \tag{22}$$

Furthermore, the diffusivity, χ, is determined by:

$$\chi = \frac{2}{3}\left(\tau_c - \frac{1}{2}\right)\delta t \tag{23}$$

Eqs. (2) and (11) should both be solved using a two-step procedure, i.e. a collision step followed by a streaming step. The streaming step requires little computational effort since it simply advances the data from the neighboring lattice points, while the collision step is completely localized.

3. Boundary Conditions Treatment in LBM

A difficulty inherent in the LBM is that the boundary conditions for the distribution function are not known beforehand. It is therefore necessary to construct suitable conditions for f_α and g_α based on the macroscopic flow variables. The simulations performed in this study consider three specific cases.

Case A: The thermal boundary condition is the same as that presented by Kondoh [13], i.e. the step-side lower wall downstream of the step is maintained at a constant temperature higher than that of the inlet temperature, while the remaining part of the wall is considered adiabatic.

Case B: A constant high inlet temperature with the walls at a constant lower temperature.

Case C: A cylinder inserted in the backward-facing step flow. The thermal boundary conditions are the same as those of case B. The inserted cylinder is assumed to be thermally isolated such that they play no role in heat transfer, but serve only to interrupt the flow. As shown in Fig. 1, the cylinder is located at a distance of $5/6H$ downstream from the step and in the middle of the y direction.

A uniform grid is used throughout the current numerical simulations. The convergence criteria in each run are as follows:

$$\frac{\sum_{i,j}\|\vec{V}(x_{i,j},t+\delta t)-\vec{V}(x_{i,j},t)\|}{\sum_{i,j}\|\vec{V}(x_{i,j},t)\|} \leqslant 1.0\times 10^{-8} \tag{24}$$

$$\frac{\sum_{i,j}\|T(x_{i,j},t+\delta t)-T(x_{i,j},t)\|}{\sum_{i,j}\|T(x_{i,j},t)\|} \leqslant 1.0\times 10^{-8} \tag{25}$$

where $\|*\|$ is the L_2 norm.

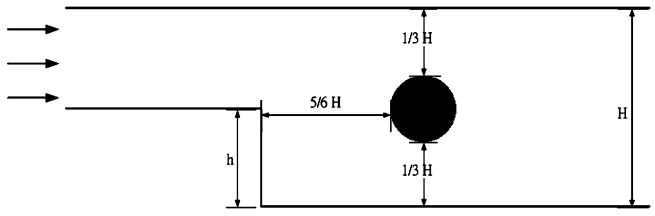

Fig. 1. Geometry of backward-facing step with a cylinder.

3.1. Boundary conditions of velocity field

A constant velocity flow of 0.05 is applied at the inlet. The velocity is specifically chosen to be less than 10% of the speed of sound to avoid generating significant compressibility effects, which are known to increase with the square of the Mach number. Using the bounce-back rule of the non-equilibrium distribution proposed by Zou and He [26], the equilibrium density distribution function is computed from the pressure and the given velocity and imposed at the first lattice column. At the outlet, a fixed pressure is imposed in terms of the equilibrium distribution function. The velocity components are extrapolated upstream.

The bounce-back rule of the non-equilibrium distribution proposed by Zou and He [26] is used for the no-slip boundary condition at the wall. The density distribution function at the boundary must satisfy the following condition:

$$f_\alpha^{\text{neq}} = f_\beta^{\text{neq}} \tag{26}$$

where e_α and e_β have opposite directions. The velocity at the wall is used when calculating f^{eq} for the boundary nodes in order to enforce the no-slip boundary condition.

3.2. Boundary conditions of temperature field

For the thermal problem, the thermal energy distribution function at the boundary satisfies:

$$g_\alpha^{\text{neq}} - e_\alpha^2 f_\alpha^{\text{neq}} = -\left(g_\beta^{\text{neq}} - e_\beta^2 f_\beta^{\text{neq}}\right) \tag{27}$$

The temperature of the wall is used when calculating g^{eq} for the boundary nodes in order to satisfy the given temperature. This study imposes Neumann and Dirichlet boundary conditions for the temperature field. For the Dirichlet type condition, the given temperature is applied directly on the boundary. Meanwhile, the Neumann type condition is transferred to the Dirichlet type condition through the conventional second-order finite difference approximation in order to obtain the temperature at the boundary [27]. When the temperature gradient is given, the temperature at the boundary can be calculated by:

$$\left.\frac{\partial T}{\partial y}\right|_{x,1} = \frac{-3T_{x,1}+4T_{x,2}-T_{x,3}}{2\Delta y} \tag{28}$$

Eq. (28) yields the corresponding Dirichlet type boundary condition for both the adiabatic and constant heat flux boundary conditions.

3.3. Boundary condition treatment of cylinder

This study applies the boundary treatment proposed by Guo [10] to the cylinder inserted in the channel downstream of the backward step. Basically, this boundary treatment decomposes the distribution function, f_α, at a wall node into equilibrium and non-equilibrium parts. The non-equilibrium part is approximated by that of the neighboring fluid node along the link, while the equilibrium part is determined by an imaginary equilibrium distribution where the boundary condition is enforced. As shown in Fig. 2, the link between the fluid node, $\vec{x}_f$,

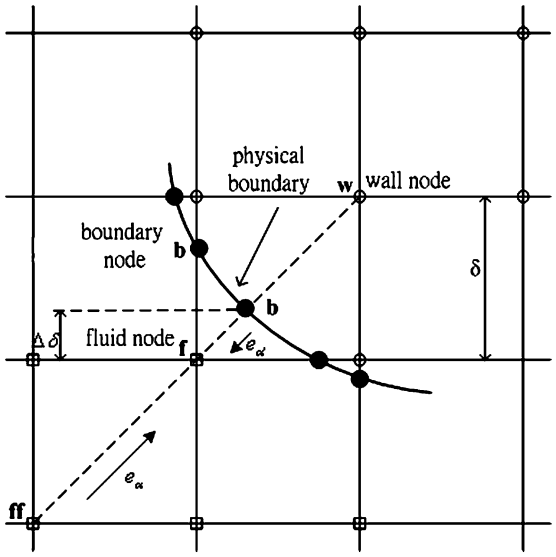

Fig. 2. Curved boundary and lattice nodes.

and the wall node, $\vec{x}_w$, intersects the physical boundary at $\vec{x}_b$. The fraction of the intersected link in the fluid region is defined as:

$$\Delta = \frac{(|\vec{x}_f - \vec{x}_b|)}{(|\vec{x}_f - \vec{x}_w|)} \tag{29}$$

In order to specify $f_\alpha(\vec{x}_w, t)$, it is necessary to decompose $f_\alpha(\vec{x}_w, t)$ into $f_\alpha^{\mathrm{eq}}(\vec{x}_w, t)$ and $f_\alpha^{\mathrm{ne}}(\vec{x}_w, t)$. Rather than using the original definition of the equilibrium density distribution given in Eq. (3), the equilibrium part, $f_\alpha^{\mathrm{eq}}(\vec{x}_w, t)$, can be defined approximately as:

$$f_\alpha^{\mathrm{eq}}(\vec{x}_w, t) = \mathrm{w}_\alpha \rho_w \left[1 + \frac{3\vec{e}_\alpha \cdot \vec{V}_w}{c^2} + \frac{9}{2}\frac{(\vec{e}_\alpha \cdot \vec{V}_w)^2}{c^4} - \frac{3}{2}\frac{\vec{V}_w^2}{c^2}\right] \tag{30}$$

where $\vec{V}_w$ is an approximation of $\vec{V}_w = \vec{V}(\vec{x}_w)$ and $\rho_w \equiv \rho(\vec{x}_f)$ is an approximation of$\rho_w = \rho(\vec{x}_w)$. It is reasonable to determine $\vec{V}_w$ via linear extrapolation using either $\vec{V}_{w1} = (\vec{V}_b + (\Delta - 1)\vec{V}_f)/\Delta$ or $\vec{V}_{w2} = (2\vec{V}_b + (\Delta - 1)\vec{V}_{ff})/(1 + \Delta)$ and $\vec{V}_w = \vec{V}_{w1} = (\vec{V}_b + (\Delta - 1)\vec{V}_f)/\Delta$ for $\Delta \geqslant 0.75$ and $\vec{V}_w = \Delta\vec{V}_{w1} + (1 - \Delta)\vec{V}_{w2}$ for $\Delta < 0.75$. Guo [10] proposed the non-equilibrium part as $f_\alpha^{\mathrm{ne}}(\vec{x}_w, t) = f_\alpha^{\mathrm{ne}}(\vec{x}_f, t)$ for $\Delta \geqslant 0.75$ and $f_\alpha^{\mathrm{ne}}(\vec{x}_w, t) = \Delta f_\alpha^{\mathrm{ne}}(\vec{x}_f, t) + (1 - \Delta) f_\alpha^{\mathrm{ne}}(\vec{x}_{ff}, t)$ for $\Delta < 0.75$. Finally, the post-collision distribution function, $f_\alpha^+(\vec{x}_w, t)$, can be obtained as:

$$f_\alpha^+(\vec{x}_w, t) = f_\alpha^{\mathrm{eq}}(\vec{x}_w, t) + (1 - 1/\tau_v) f_\alpha^{\mathrm{ne}}(\vec{x}_w, t) \tag{31}$$

The thermal boundary condition of the cylinder is adiabatic. Based on the fraction of the intersected link in the fluid region Δ, the temperature of $\vec{x}_f$ can be approximated by interpolation of the neighboring points.

4. Results and discussions

4.1. Overview of velocity field

The simulations in the current study were performed using a uniform rectangular mesh (801 × 61). The channel expansion ratio (*ER*) was defined as H/h (see Fig. 1) and the Reynolds number (*Re*) of the flow as $4U(H-h)/3\nu$, where U is the maximum velocity in the inlet. The velocity vector plots in Fig. 3(a), corresponding to the case where the cylinder is not present in the flow, provide an overall view of the flow for $ER = 2$ and $Re = 170$. As expected in a backward-facing step flow, a recirculation zone is formed behind the step. The location of the reattachment point is found to be $X_R/h = 3.18$ and 5.5 at Reynolds numbers of $Re = 100$ and 200, respectively. These results differ from the experimental findings of Armaly et al. [12], who reported reattachment locations of $X_R/h = 3.1$ and 5.4 at $Re = 100$ and 200, respectively. The discrepancy between the two sets of results can be attributed to the slight difference in the geometric configuration of the flow. However, the present numerical results are similar to those of He [28], i.e. $X_R/h = 3.15$ at $Re = 100$. As expected, with increasing Reynolds number the length of flow redevelopment downstream of the step increased.

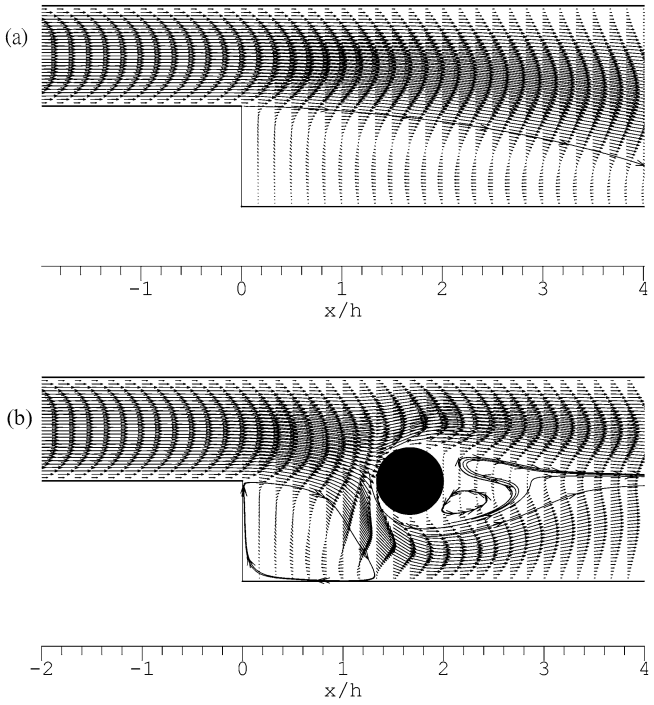

Fig. 3. Velocity field ($ER = 2$, $Re = 170$) for: (a) no obstacle, (b) with a cylinder.

Figs. 3(b) show the velocity vector fields when a cylinder is inserted into the channel. It is apparent that the introduction of the cylinder causes a narrowing of the main recirculation region as a result of the interruption within the flow. There also has a small recirculation zone behind the cylinder. The overall flow structure is in good agreement with that predicted intuitively.

4.2. Overview of temperature field

Case A imposes the same boundary condition as that considered by Kondoh [13]. Fig. 4 shows the influence of the Reynolds number on the local heat transfer coefficient distribution on the heat transfer surface for conditions of $ER = 1.5$ and $Pr = 0.7$. It can be seen that as the Reynolds number increases, the peak value of *Nu* not only increases, but also moves downstream. The downstream shift of this peak value is most likely related

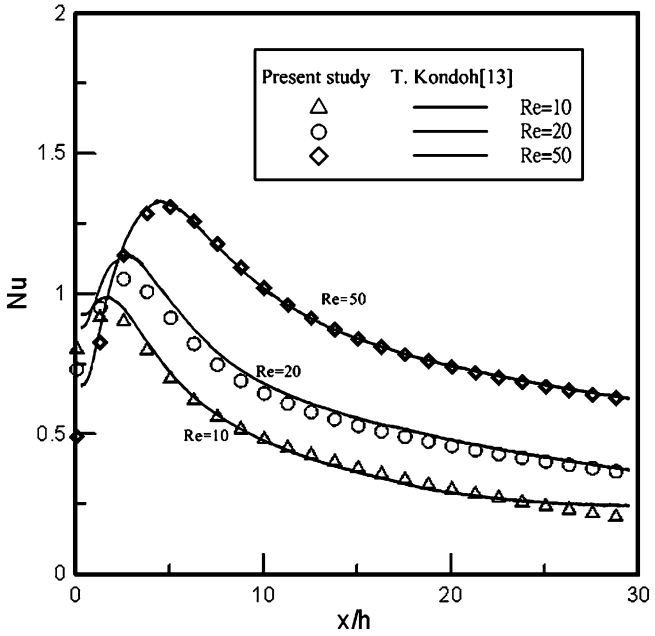

Fig. 4. Comparison of present Nusselt number results with those of Kondoh [13] for case A ($ER = 1.5$, $Pr = 0.7$).

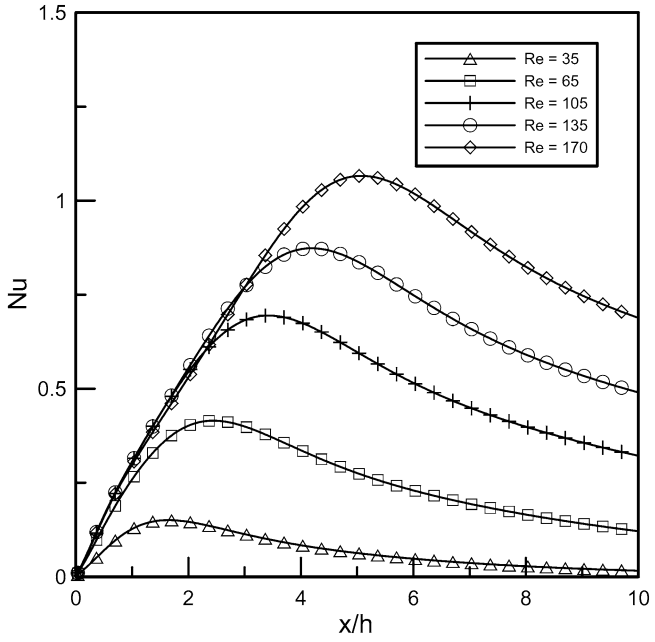

Fig. 5. Effect of Reynolds number on Nusselt number for case B ($ER = 2$, $Pr = 0.7$).

to a corresponding movement of the flow attachment length. From Fig. 4, it is clear that the present numerical data are in good agreement with the results of Kondoh [13] other than in the vicinity of the step.

Fig. 5 shows the influence of the Reynolds number on the local heat transfer coefficient distribution on the heat transfer surface for case B (a constant temperature wall boundary condition). Although the results display a broadly similar trend to those shown in Fig. 4, the results obtained for the Nusselt number are somewhat different near the step because of the different thermal boundary conditions applied. Due to the different thermal boundary condition and Reynolds number definition, the corresponding Nusselt number is also different. But the movement of the peak values of Nusselt number still related to the movement of the flow attachment length.

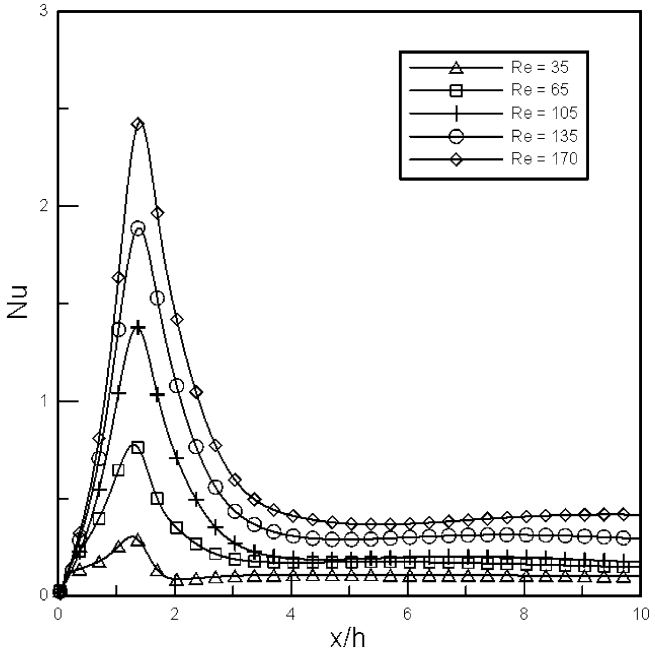

Fig. 6. Effect of Reynolds number on Nusselt number for case C with a cylinder ($ER = 2$, $Pr = 0.7$).

Fig. 6 shows the influence of the Reynolds number on the local heat transfer coefficient distribution for case C, with a cylinder inserted in the flow. It can be seen that the local *Nu* values are higher than in the case when no obstacles are present in the flow. In other words, the convective heat transfer performance is improved. The presence of the cylinder in the flow changes the velocity field and compresses the thermal boundary layer, which enhances the heat transfer. The enhancement effect is particularly evident at higher Reynolds numbers.

Fig. 7 shows the variation of the average Nusselt number with the Reynolds number with and without the cylinder. It is observed that the cylinder enhance the thermal performance, particularly when the Reynolds number is high. From inspection, the thermal performance is found to increase by approximately 33% at $Re = 170$.

4.3. Numerical verification of field synergy principle

Three mechanisms are responsible for enhancing the single-phase convective heat transfer, namely an increased flow interruption, a reduced thermal boundary layer thickness, and an increased velocity gradient near the solid wall [18]. These three mechanisms lead to a reduction of the intersection angle between the velocity vector and the temperature gradient. This section of the paper compares cases B and C to illustrate the inherent relation between the field synergy principles and to demonstrate that increasing the flow interruption enhances the single phase convective heat transfer. It also indicates that the heat transfer rate depends not only on the flow and temperature fields, but also on their synergy.

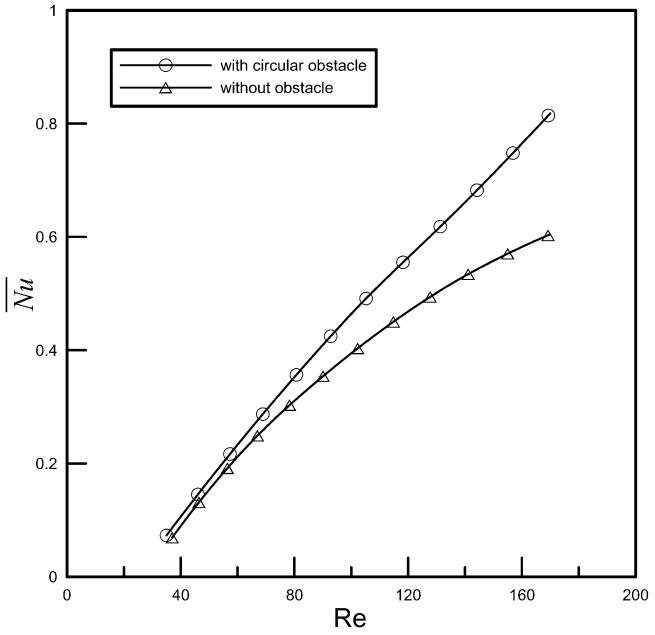

Fig. 7. Effect of Reynolds number on average Nusselt number with and without a cylinder.

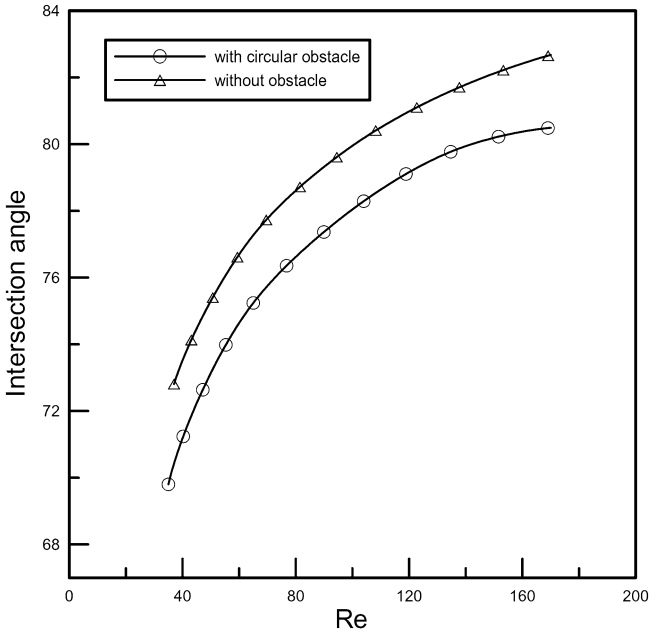

Fig. 8. Effect of Reynolds number on average intersection angle with and without a cylinder.

Base on an analog between the heat conduction and heat convection mechanism, convection heat transfer is essentially the heat conduction with fluid motion [16,17,29]. Eq. (32) which derived from [16,17] provides a general insight into convective heat transfer. This equation suggests that the heat transfer can be enhanced in one of three ways, namely increasing the Reynolds and Prandtl numbers, increasing the fullness of the dimensionless velocity and temperature profiles, and increasing the intersection angle between the dimensionless velocity and temperature gradient vectors:

$$Re\,Pr\int(\vec{V}\cdot\nabla T)\,\mathrm{d}y = Nu \tag{32}$$

$$\vec{V}\cdot\nabla T = |\vec{V}||\nabla T|\cos\theta \tag{33}$$

where in Eq. (33) θ is the intersection angle and θ_m is the average intersection angle between the velocity vector and the temperature gradient in the computation domain. If the local value of θ is greater than 90°, its value is taken as $(180^\circ - \theta)$ when added to the summation of the intersection angle [18]. Fig. 8 shows the variation of the average intersection angle with *Re* both with and without the cylinder. An enhanced synergy is obtained by decreasing the intersection angle between the velocity vector and the temperature gradient. From Fig. 8, it is seen that this can be achieved by increasing the interruption within the flow. As the intersection angle reduces by approximately 3 degrees, the average Nusselt number increases by approximately 33% for Reynolds numbers below $Re = 170$. If the concept of the field synergy principle does not apply to heat transfer, the only indicator of the heat transfer performance is the Nusselt number. However, the synergy principle provides an alternative index for evaluating the heat transfer performance. In the theory, the optimal heat transfer can be obtained at an intersection angle of 0 degrees. In practice, the intersection angle is determined by the geometry of the channel and the boundary conditions imposed. So the field synergy principle is a new direction to assess the heat transfer performance.

5. Conclusions

This study has simulated low Reynolds number backward-facing step flows using a single-relaxation-time model based on the D2Q9 LBM model. The numerical results obtained for the velocity and temperature fields are in good agreement with the published experimental and numerical results. The simplified thermal model applied in this paper is easy to use and indeed an appropriate LBM thermal model for performing accurate simulations of incompressible thermal fluid flows. The results have shown that inserting cylinder enhances the convective heat transfer as a result of flow interruption and thermal boundary layer compression effects. The results have indicated that increasing the cylinder is beneficial in enhancing the heat transfer and leads to a reduction in the intersection angle between the velocity vector and the temperature gradient.

References

[1] S. Chen, G.D. Doolen, Lattice Boltzmann method for fluid flows, Annu. Rev. Fluid Mech. 30 (1998) 329–364.
[2] G. McNamara, G. Zanetti, Use of the Boltzmann equation to simulate Lattice–Gas automata, Phys. Rev. Lett. 61 (1988) 2332–2335.
[3] F. Higuera, J. Jimenez, Boltzmann approach to lattice gas simulations, Europhys. Lett. 9 (1989) 663–668.
[4] F. Higuera, S. Succi, R. Benzi, Lattics gas dynamics with enhanced collisions, Europhys. Lett. 9 (1989) 345–349.
[5] P.L. Bhatnagar, E.P. Gross, M. Krook, A model for collision process in gases. I. Small amplitude processes in charged and neutral one-component system, Phys. Rev. 94 (1954) 511–521.

[6] H. Chen, S. Chen, W.H. Matthaeus, Recovery of the Navier–Stokes equation using a lattice Boltzmann method, Phys. Rev. A 45 (1992) 5339–5342.

[7] Y.H. Qian, D. d'Humiéres, P. Lallemand, Lattice BGK models for Navier–Stokes equation, Europhys. Lett. 17 (1992) 479–484.

[8] O. Filippova, D. Hanel, Grid refinement for lattice-BGK models, J. Comput. Phys. 147 (1998) 219–228.

[9] R. Mei, L.-S. Luo, W. Shyy, An accurate curved boundary treatment in the lattice Boltzmann method, J. Comput. Phys. 155 (1999) 307–330.

[10] Z. Guo, C. Zheng, B. Shi, An extrapolation method for boundary conditions in lattice Boltzmann method, Phys. Fluids 14 (2002) 2007–2010.

[11] S. Chen, D. Martinez, R. Mei, On boundary conditions in lattice Boltzmann methods, Phys. Fluids 8 (1996) 2527–2536.

[12] B.F. Armaly, F. Durst, J.C.F. Pereira, B. Schonung, Experimental and theoretical investigation of backward-facing step flow, J. Fluid Mech. 127 (1983) 473–496.

[13] T. Kondoh, Y. Nagano, T. Tsuji, Computational study of laminar heat transfer downstream of a backward-facing step, Int. J. Heat Mass Transfer 36 (1993) 577–591.

[14] W. Aung, An experimental study of laminar heat transfer downstream of backstep, J. Heat Transfer 105 (1983) 823–829.

[15] E.J. Hall, R.H. Pletcher, An application of a viscous-inviscid interaction procedure to predict separated flows with heat transfer, J. Heat Transfer 107 (1985) 557–563.

[16] Z.Y. Guo, D.Y. Li, B.X. Wang, A novel concept for convective heat transfer enhancement, Int. J. Heat Mass Transfer 41 (5) (1998) 2221–2225.

[17] S. Wang, Z.X. Li, Z.Y. Guo, Novel concept and device of heat transfer augmentation, in: Proceeding of 11th IHTC 5, 1998, pp. 405–408.

[18] W.Q. Tao, Y.L. He, Q.W. Wang, Z.G. Qu, F.Q. Song, A unified analysis on enhancing single phase convective heat transfer with field synergy principle, Int. J. Heat Mass Transfer 45 (2002) 4871–4879.

[19] W.Q. Tao, Z.Y. Guo, B.X. Wang, Field synergy principle for enhancing convective heat transfer—its extension and numerical verifications, Int. J. Heat Mass Transfer 45 (2002) 3849–3856.

[20] Z.Y. Guo, W.Q. Tao, R.K. Shah, The field synergy (coordination) principle and its applications in enhancing single phase convective heat transfer, Int. J. Heat Mass Transfer 48 (2005) 1797–1807.

[21] S. Hou, Q. Zou, S. Chen, G.D. Doolen, A.C. Cogley, Simulation of cavity flow by the lattice Boltzmann method, J. Comput. Phys. 118 (1995) 329–347.

[22] F.J. Alexander, S. Chen, J.D. Sterling, Lattice Boltzmann thermohydrodynamics, Phys. Rev. E 47 (1993), R2249.

[23] X. Shan, Solution of Rayleigh–Benard convection using a lattice Boltzmann method, Phys. Rev. E 55 (1997) 2780–2788.

[24] X. He, S. Chen, G.D. Doolen, A novel thermal model for the lattice Boltzmann method in incompressible limit, J. Comput. Phys. 146 (1998) 282–300.

[25] Y. Peng, C. Shu, Y.T. Chew, Simplified thermal lattice Boltzmann model for incompressible thermal flows, Phys. Rev. E 68 (2003) 026701.

[26] Q. Zou, X. He, On pressure and velocity boundary conditions for the lattice Boltzmann BGK model, Phys. Fluids 9 (1997) 1591–1598.

[27] C. Shu, Y. Peng, Y.T. Chew, Simulation of natural convection in a square cavity by Taylor series expansion and least square-based lattice Boltzmann method, Int. J. Modern Phys. C 13 (2002) 1399–1414.

[28] X. He, L.-S. Luo, A prior derivation of the lattice Boltzmann equation, Phys. Rev. E 55 (1997) 6333–6336.

[29] F.M. White, Heat Transfer, Addison-Wesley, New York, 1984.